Int. J. Electrochem. Sci., 13 **(2018)** 8454 – 8470, doi: 10.20964/2018.09.72

International Journal of
ELECTROCHEMICAL
SCIENCE
www.electrochemsci.org

A Nonenzymatic Sensor Based on {PEI/[$P_2W_{17}V$-CNTs/PEI-CuO]$_{10}$/$P_2W_{17}V$-CNTs} Nanocomposite Film for the Sensitive Determination of Iodate

Xinming Wang[1], *Yuanqing Zhao*[1], *Di Zhang*[1,2], *Li Zhang*[1], *Zhenyuan Bai*[1], *Haijun Pang*[1], *Huiyuan Ma*[1,*]

[1] Key Laboratory of Green Chemical Engineering and Technology of College of Heilongjiang Province, College of Chemical and Environmental Engineering, Harbin University of Science and Technology, Harbin 150040, China
[2] School of Materials Science and Engineering, Harbin Institute of Technology, Harbin 150001, China
[*]E-mail: mahy017@163.com

Received: 6 May 2018 / *Accepted:* 11 July 2018 / *Published:* 5 August 2018

In this work, a new composite film electrode based on Dawson-type polyoxometalate α_2-$K_7P_2VW_{17}O_{62}\cdot 18H_2O$ ($P_2W_{17}V$) and accessory copper oxide nanoparticles (CuO NPs) with a composite of carbon nanotubes (CNTs) was successfully proposed and employed for iodate (IO_3^-) analysis. Highly stable determination of IO_3^- was achieved by a combination of cyclic voltammetric and chronoamperometric methods performed on this layer-by-layer (LbL) self-assembly composite film electrode. For the tricomponent composite film, the amperometric response time of iodate (defined as the time to achieve 95% steady-state current) was estimated to be 2 s, confirming the faster electron transfer rate in the tricomponent composite film. This iodate sensor with 10 bilayers has a linear range of 1.25×10^{-7} to 1.63×10^{-4} M, a low detection limit of 1.5×10^{-8} M (S/N = 3), a high sensitivity of 4.82 mA mM^{-1} IO_3^- and an excellent anti-interference performance. In addition, the composite film could also be applied to detect iodate in table salt. The as-prepared sensor can be used for detecting iodate with a good average recovery of 100.1%, indicating the well reliability of the present sensor for iodate determination in table salts. This approach may open a new path for the rational design of high-performance tricomponent composite film electrochemical sensors.

Keywords: polyoxometalate; modified electrode; composite film; iodate sensor

1. INTRODUCTION

As an essential element, iodine is an indispensable requirement for the synthesis of thyroid hormones, thyroxine (T4), and triiodothyronine (T3) [1, 2]. From the announcement of the World

Health Organization (WHO), the majority of mental retardation on a global scale is led by iodine deficiency. In general, iodized salt is considered to be an effective way to prevent iodine deficiency disorder. Nevertheless, excessive intake of iodine will cause goiter and hypothyroidism, as well as hyperthyroidism. Accordingly, the detection of iodine in table salt is important for successful complement of iodine. Recently, many analytical techniques have been developed for the detection of iodate, including chromatography [3–5], fluorescence quenching [6], and flow injection analysis [7, 8]. However, these referred methods require time-consuming sample pretreatment and expensive reagents. Therefore, it is of great necessity to develop a simple and easily recyclable sensor for the detection of iodate. Electrochemical techniques have been developed as an effective method for iodate determination because of their easy operation, low cost and high sensitivity.

Because the temperature, pH and humidity could easily influence the accuracy of traditional enzyme-based biosensors, researchers have developed a mass of chemosensors by utilizing supramolecular chemistry, which allows one to rationally design new anion-responsive receptors with agreeable or even remarkable selectivities [9–12] and that are capable of recognizing, sensing, and separating negatively charged species. As a coin has two sides, the utilization of chemosensors has its own share of controversy, for instance, the intricate organic synthesis procedure involved, the water-incompatible properties, and a rather high limit of detection[13–15]. In comparison with mature chemosensors, much more interest should focus on multicomponent, nanohybrid electrochemical sensors.

Polyoxometalates (POMs) possess both redox and electrochemical behavior [16–20]. These structurally well-defined POM clusters are suitable as excellent electrocatalysts, which can undergo a reversible, fast, stepwise redox multi-electron transfer process [21]. Compared to traditional POMs, vanadium-substituted POMs can increase the negative charge of the obtained anions, and this increase is beneficial for subsequent deposition of active species [22, 23]. Diana M. Fernandes et al. investigated the electrocatalytic activity of hybrid multilayer films based on Keggin-type polyoxometalate $K_5[PMo_{11}VO_{40}]$ ($PMo_{11}V$) andpararosaniline (PR). For the reduction of iodate and ascorbic acid oxidation, they exhibited excellent electrocatalytic activity [24]. Luís Cunha-Silva and co-workers prepared a novel hybrid composite material polyoxovanadate@MIL-101(Cr) ($PMo_{10}V_2$@MIL-101), which showed efficient electrocatalytic activity for ascorbic acid oxidation [25]. In recent years, our group fabricated some composite films based on vanadium-substituted polyoxometalates and investigated their electrocatalytic properties in electrochemical sensors [26–29].

As promising candidates for sensors, transition metals and their oxides have been explored [30]. CuO is an interesting material among these materials for sensors. It is non-toxic, inexpensive, and stable. Above all, CuO is a p-type semiconductor with a narrow band gap of 1.2 eV, and CuO nanomaterials have shown increased catalytic activity [31–32]. Great efforts have been made to combine carbon-based nanomaterials, such as carbon nanotubes with copper oxides, to enhance the catalytic activity and avoid the aggregation of nanomaterials [33]. Based on carbon-based nanomaterials, the modified electrodes possess the advantages of wide linear range, high sensitivity, good stability, low detection limit, and reproducibility [34–45].

Considering all of the above, we propose a facile method to prepare tricomponent nanocomposite based on α_2-$K_7P_2VW_{17}O_{62}\cdot 18H_2O$ ($P_2W_{17}V$), CNTs, and CuO. The introduction of

CuO NPs and CNTs played an important role in enhancing the conductivity. The $P_2W_{17}V$-CNTs-CuO nanocomposite film modified electrode was employed for electrochemical sensing of IO_3^-. For the tricomponent composite film, the amperometric response time of iodate (defined as the time to achieve 95% steady-state current) was estimated to be 2 s, confirming the faster electron transfer rate in the tricomponent composite film. Due to the low operating potential in the electrocatalytic reduction process, there was also no effect on the as-prepared sensor to determine IO_3^- when interference was added. The relatively high stability along with the excellent reproducibility makes it available for the determination of iodate. The as-prepared sensor can efficiently be used for detecting iodate with a good average recovery of 100.1%, indicating the reliability of the present sensor for iodate determination in table salts.

2. EXPERIMENTAL SECTION

2.1 Reagents

α_2-$K_7P_2VW_{17}O_{62}\cdot 18H_2O$ was prepared in accordance with the literature [46, 47] and verified by UV-vis spectroscopy and cyclic voltammetry. Poly(ethylenimine) (PEI MW 750,000) was bought from Aldrich and utilized as received. CNTs were obtained from Prof. Yongfu Liang at the College of Materials Chemistry and Chemistry Engineering, Heilongjiang University. Other reagents were of analytical grade. The copper oxide nanoparticles were prepared according to the reported literature [48]. Figure 1 presents the TEM image of CuO NPs.

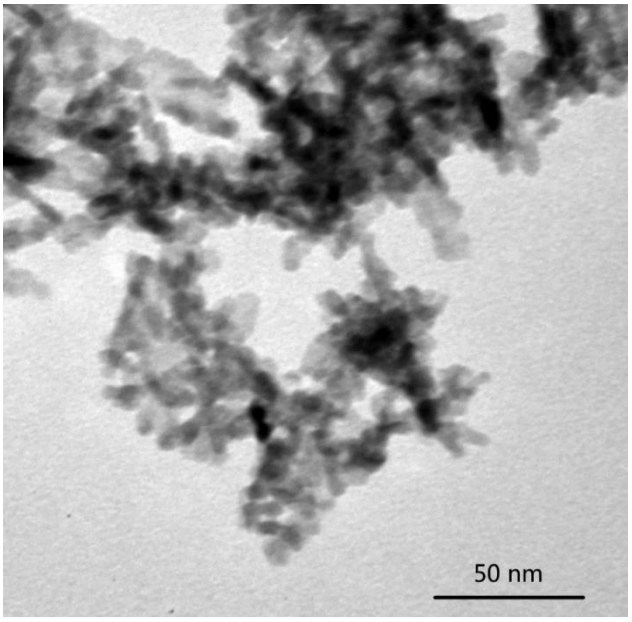

Figure 1. TEM image of the CuO NPs.

2.2 Fabrication of the layer-by-layer composite film

The fabrication procedure of the multilayer assemblies of alternating $P_2W_{17}V$-CNTs and CuO

NPs is schematically illustrated in Scheme 1. A pre-cleaned glass substrate was first immersed in a protonic PEI (10 mM) aqueous solution to form a precursor. Based on the electrostatic interaction, the PEI-coated substrate was successively immersed in a negatively charged $P_2W_{17}V$-CNTs (1.0 mg/mL CNTs + 3.0 mg/mL $P_2W_{17}V$) solution and a positively charged CuO NPs solution. After repeating the dipping cycles several times, a desired composite film with *n* layers of $[P_2W_{17}V\text{-CNTs/PEI-CuO}]_n$ is obtained. For comparison, the two-component films $[P_2W_{17}V\text{-CNTs/PEI}]_n/P_2W_{17}V\text{-CNTs}$ and $[P_2W_{17}V\text{/PEI-CuO}]_n/P_2W_{17}V$ were prepared under the same condition.

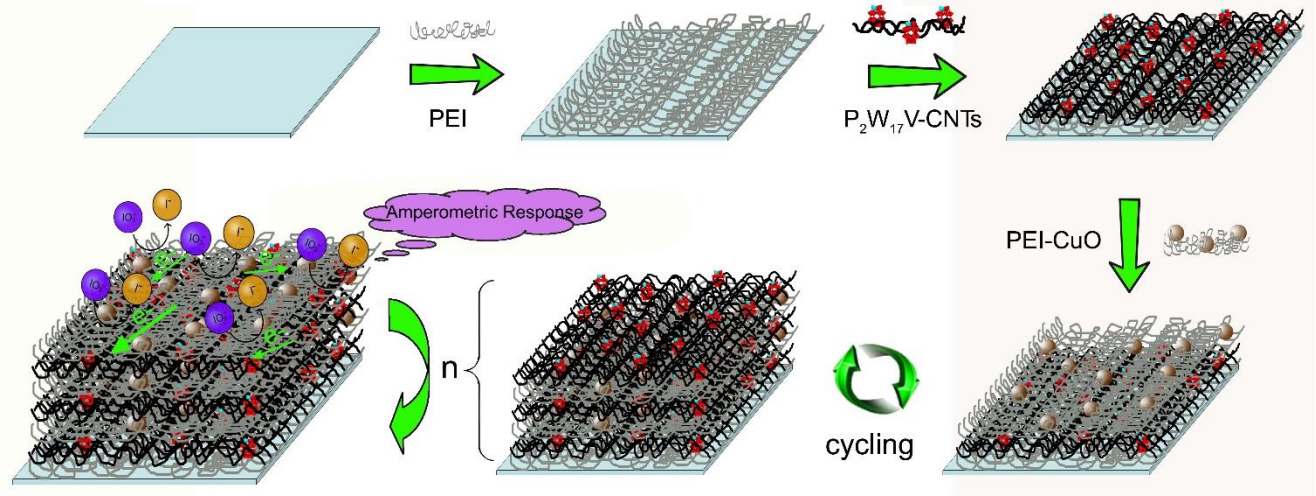

Scheme 1. Preparation routes of the as-prepared sensor.

2.3 Characterization and electrochemical measurements

Using a U-3900 UV-vis spectrophotometer (Hitachi, Japan), UV-vis absorption spectra were recorded. By using a Dimension TM3100 series AFM produced by Digital Instruments (Santa Barbara, California, USA), atomic force microscopy (AFM) images were taken. With an accelerating voltage of 100 kV, transmission electron microscopy (TEM) was performed on a JEOL-1400. The TEM samples were prepared by drop-casting the dispersion onto copper grids covered by carbon film. Using Mg Kα X-ray radiation as the X-ray source for excitation, X-ray photoelectron spectra (XPS) were obtained on an ESCALAB-MKII spectrometer.

A CHI760D Electrochemical Workstation (Shanghai Chenhua Instrument Corporation, China) was used to carry out the electrochemical experiments. With a tricomponent composite film as a working electrode, a twisted platinum wire as a counter electrode, and Ag/AgCl as a reference electrode, a conventional three-electrode system was adopted.

3. RESULTS AND DISCUSSION

3.1 UV-vis spectra

The consecutive process of growth of the composite film $[P_2W_{17}V\text{-CNTs/CuO}]_n/P_2W_{17}V\text{-CNTs}$

(with n = 2, 4, 6, 8 and 10) was monitored by UV-vis spectroscopy, where the increasing absorption can be assigned to the cumulative layering of $P_2W_{17}V$-CNTs and CuO NPs, as shown in Figure 2(a). It is clear that the tricomponent composite film $[P_2W_{17}V\text{-CNTs/CuO}]_n/P_2W_{17}V\text{-CNTs}$ (n = 2, 4, 6, 8 and 10) exhibits two characteristic absorption peaks at approximately 200 and 276 nm in the UV region. The first is due to the terminal oxygen to tungsten ($O_d \rightarrow W$) charge transfer transition, and the latter is the overlap of $P_2W_{17}V$ and CuO NPs bands (see Figure 2(b)). The nearly linear increase in the peak absorbance at 200 and 276 nm with the number of layers in $P_2W_{17}V$-CNTs/CuO, as shown in the inset of Figure 2(a), indicates that the growth for each absorption cycle is uniform and stable in terms of LbL growth. Figure 2(b) displays the UV-vis spectra of $P_2W_{17}V$ solution, CuO nanoparticles, two-component composite film $[P_2W_{17}V/CuO]_{10}/P_2W_{17}V$ and the tricomponent composite film $\{PEI/[P_2W_{17}V\text{-CNTs/PEI-CuO}]_{10}/P_2W_{17}V\text{-CNTs}\}$. In this figure, it can be seen that these two characteristic absorption peaks of tricomponent composite film $[P_2W_{17}V\text{-CNTs/CuO}]_{10}/P_2W_{17}V\text{-CNTs}$ (at 200 and 276 nm) and two-component composite film $[P_2W_{17}V/CuO]_{10}/P_2W_{17}V$ (at 197 and 284 nm) have a different degree of a slight shift in comparison with that of $P_2W_{17}V$ solution. Moreover, the shift degree of the tricomponent composite film is larger than that of the two-component composite film. This shift degree could be due to the stronger interaction between $P_2W_{17}V$-CNTs and CuO NPs than that between $P_2W_{17}V$ and CuO NPs. Furthermore, due to the promoted quantity of absorbed CNTs in the tricomponent composite film, the absorption value of the tricomponent composite film in the range of 400-800 nm is greater compared to that of the two-component composite film $[P_2W_{17}V/CuO]_{10}/P_2W_{17}V$.

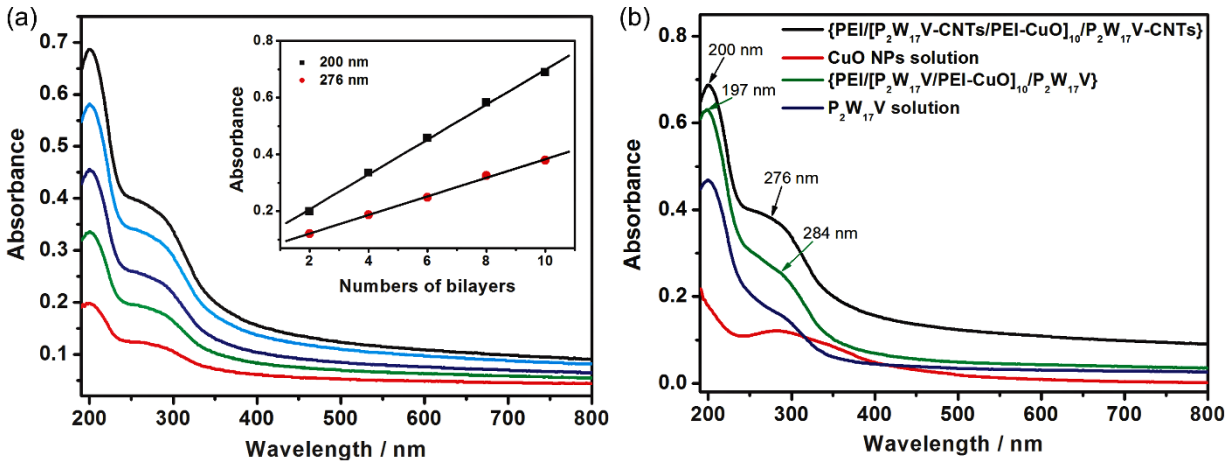

Figure 2. (a) UV-vis absorption spectra of the three-component composite film $\{PEI/[P_2W_{17}V\text{-CNTs/PEI-CuO}]_n/P_2W_{17}V\text{-CNTs}\}$ on quartz substrate with n = 2, 4, 6, 8 and 10. (b) UV-vis spectra of $P_2W_{17}V$ solution, CuO nanoparticles, two-component film $\{PEI/[P_2W_{17}V/PEI\text{-CuO}]_{10}/P_2W_{17}V\}$ and the three-component composite film $\{PEI/[P_2W_{17}V\text{-CNTs/PEI-CuO}]_{10}/P_2W_{17}V\text{-CNTs}\}$.

According to the UV-vis spectra, the surface coverage (Γ) of $P_2W_{17}V$ can be calculated by the following equation [49, 50, 51]:

$$\Gamma = \frac{N_A A_{n\lambda}}{2n\varepsilon_\lambda} \quad \text{(a)}$$

where N_A is Avogadro's constant, ε_λ is the molar extinction coefficient (M^{-1} cm^{-1}), $A_{n\lambda}$ is the absorbance at a given wavelength λ, and n is the amount of bilayer. The average surface coverage calculated from the UV-vis spectra is ca. 6.0818×10^{-10} mol/cm^2.

3.2 AFM and XPS

Figure 3 illustrates the AFM image of the three-layer tricomponent composite film $[P_2W_{17}V$-CNTs/CuO$]_3/P_2W_{17}V$-CNTs. From the AFM image, it can be seen clearly that the surface of the tricomponent composite film was covered by some evenly distributed protuberant peaks, and the particle size and root-mean-square (rms) roughness of the tricomponent composite film are 11.3 and 8.41 nm (1.0 μm × 1.0 μm), respectively.

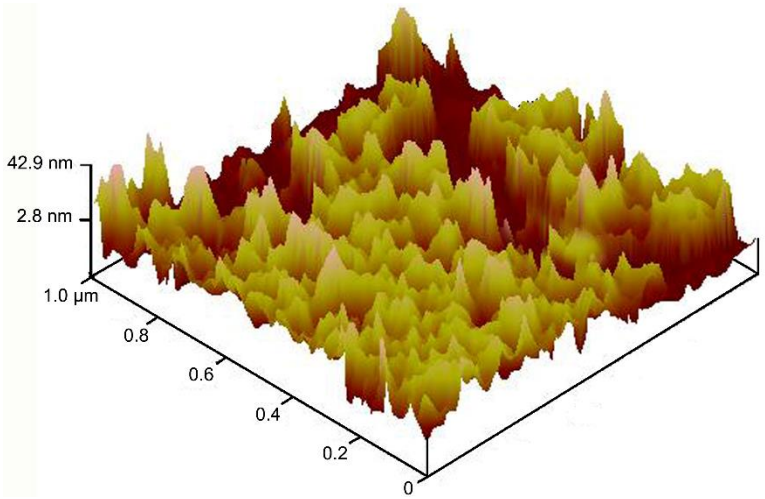

Figure 3. AFM image of the three-component composite film {PEI/$[P_2W_{17}V$-CNTs/PEI-CuO$]_3/P_2W_{17}V$-CNTs} on the silicon wafer.

The chemical composition of the resulting composite film was investigated by XPS. The XPS spectra of the tricomponent composite film $[P_2W_{17}V$-CNTs/CuO$]_3/P_2W_{17}V$-CNTs are given in Figure 4. The peaks of $W4f_{7/2}$, $W4f_{5/2}$, $V2p_{3/2}$ and $V2p_{1/2}$ are at 37.6, 35.4, 516.4 and 522.9 eV, as expected for $P_2W_{17}V$ (Figure 4 (a) and (b)). The Cu2p XPS spectrum displays two peaks at 934.0 and 954.2 eV, which can be attributed to the doublet of $Cu2p_{3/2}$ and $Cu2p_{1/2}$, respectively (Figure 4 (c)). The N1s (BE = 399.8 eV) signals are assigned to the oxidation state of nitrogen of PEI (Figure 4 (d)). From the certification of the XPS results, it could be ensured that the tricomponent composite film has been incorporated with $P_2W_{17}V$ and CuO NPs successfully.

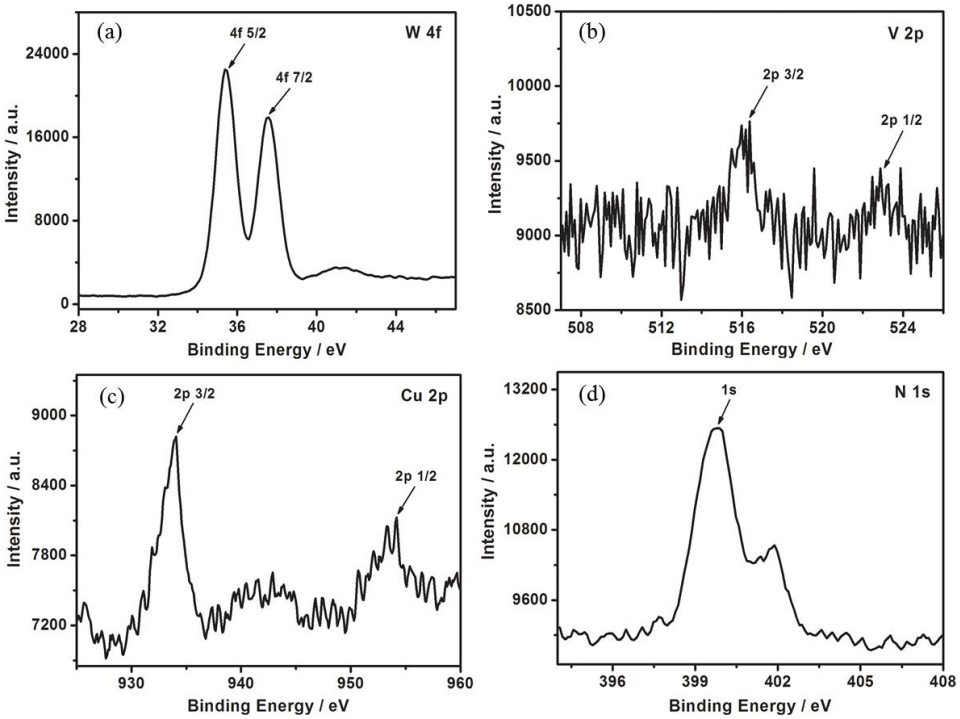

Figure 4. XPS spectra of the three-component composite film {PEI/[P_2W_{17}V-CNTs/PEI-CuO]$_3$/P_2W_{17}V-CNTs}.

3.3 The electrochemical behavior of the composite film

The electrochemical behavior of the tricomponent composite film was investigated by CV technology. Figure 5 (a) shows the cyclic voltammetric responses of the tricomponent composite film [P_2W_{17}V-CNTs/CuO]$_{10}$/P_2W_{17}V-CNTs at different scan rates ranging from 100 to 450 mV s^{-1}. It can be found that the redox peak currents gradually increased with increasing scan rate. Moreover, both the anodic peak current and cathodic peak current were linearly scaled with the scan rates in the range of 100-450 mV s^{-1} with correlation coefficient $R_a^2 = 0.9982$ for the anodic peak and $R_c^2 = 0.9996$ for the cathodic peak, which indicates a surface-confined electrochemical process (peak III, inset in Figure 5 (a)). Therefore, the surface coverage (Γ) of P_2W_{17}V can be calculated according to the equation [52]:

$$\Gamma = \frac{4i_pRT}{n^2F^2vA} \qquad \text{(b)}$$

where i_p is the peak current (A), n is the number of electrons transferred per electroactive species, v is the scan rate (V s^{-1}), A is the geometric area of the working electrode (cm^2), R is the molar gas constant, T is thermodynamic temperature and F is Faraday constant. Therefore, the surface coverage of P_2W_{17}V per layer amounts to 6.958×10^{-10} mol/cm^2. This result is in agreement with the value of 6.0818×10^{-10} mol/cm^2 measured by UV-vis spectroscopy.

The CV of P_2W_{17}V aqueous solution (in 0.5 M H_2SO_4/Na_2SO_4 solution, pH = 2.5) displays four couples of regular redox peaks in the potential range from -1.0 to 0.9 V (see Figure 5 (b)). The first pair of peaks corresponds to the one-electron redox process of V center [53], and the pairs II′, III′ and IV′ correspond to the three two-electron redox processes of W center. Compared to P_2W_{17}V aqueous

solution, the CV of the tricomponent composite film $[P_2W_{17}V\text{-CNTs/CuO}]_{10}/P_2W_{17}V\text{-CNTs}$ displays similar but more significant redox peaks, which verifies that the electrochemical property of $P_2W_{17}V$ is fully maintained in the tricomponent composite film and the incorporation of CNTs and CuO NPs into the composite films greatly improves the electrochemical response of the $P_2W_{17}V$-based composite films.

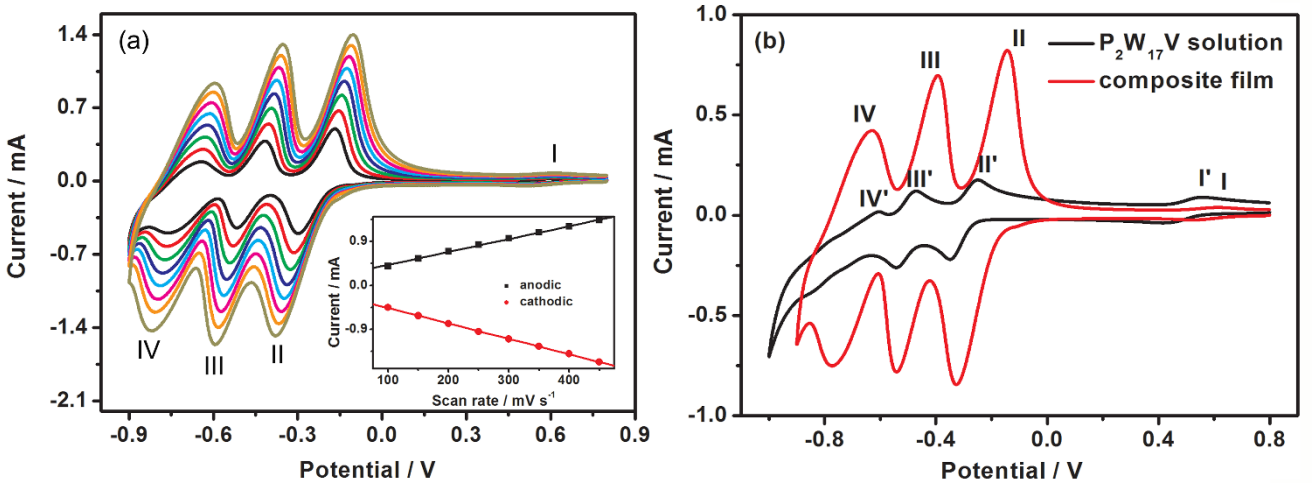

Figure 5. (a) CV curves of three-component composite film {PEI/$[P_2W_{17}V\text{-CNTs/PEI-CuO}]_{10}/P_2W_{17}V\text{-CNTs}$} in pH 2.5 H_2SO_4/Na_2SO_4 at different scan rates (0.1, 0.15, 0.2, 0.25, 0.3, 0.4 and 0.45 V s^{-1}). (b) CV curves of $P_2W_{17}V$ in solution and the three-component composite film {PEI/$[P_2W_{17}V\text{-CNTs/PEI-CuO}]_{10}/P_2W_{17}V\text{-CNTs}$}. Reference electrode: Ag/AgCl.

3.4 Electrochemical impedance spectroscopy analysis

To estimate the migration of the interface charge, electrochemical impedance spectroscopy (EIS) was conducted. Figure 6 shows the EIS Nyquist plots of the tricomponent composite film $[P_2W_{17}V\text{-CNTs/CuO}]_{10}/P_2W_{17}V\text{-CNTs}$ and two-component composite films {PEI/$[P_2W_{17}V/\text{PEI-CuO}]_{10}/P_2W_{17}V$} and $[P_2W_{17}V\text{-CNTs/PEI}]_{10}/P_2W_{17}V\text{-CNTs}$. The reaction rate on the surface of the electrode could be indicated by the arc radius of the EIS Nyquist plot. A higher efficiency of charge migration across the electrode/electrolyte interface would have a smaller arc radius. Compared to the two-component composite films, the tricomponent composite film possessed a smaller arc radius at lower frequency, suggesting that the migration of the interface charge is more efficient on the tricomponent composite film $[P_2W_{17}V\text{-CNTs/CuO}]_{10}/P_2W_{17}V\text{-CNTs}$, which further confirms that the incorporation of CNTs and CuO NPs can promote the interface charge migration. The equivalent circuit (inset of Figure 6) of the electrode system was constructed to analyze the impedance spectra, and the impedance spectra were fitted by the Zview software. R_1 is the resistance of charge transfer, R_s is the ohmic resistance of the electrolyte solution and *CPE*1 is the constant phase element.

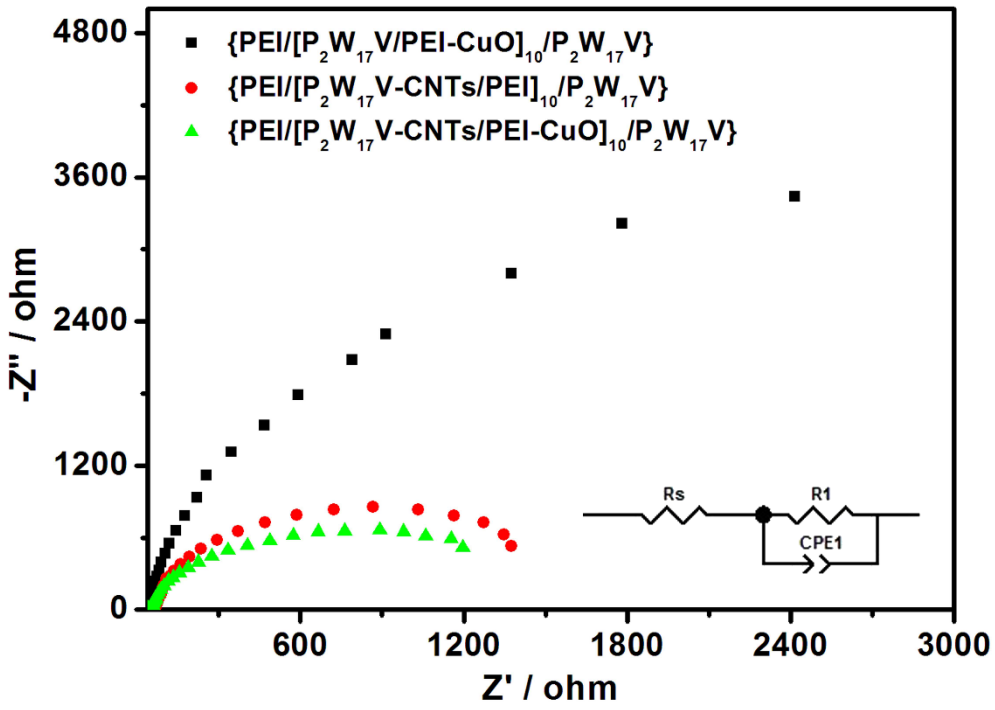

Figure 6. The EIS figure of the three-component composite film {PEI/[$P_2W_{17}V$-CNTs/PEI-CuO]$_{10}$/$P_2W_{17}V$-CNTs} and two two-component composite films {PEI/[$P_2W_{17}V$/PEI-CuO]$_{10}$/$P_2W_{17}V$} and {PEI/[$P_2W_{17}V$-CNTs/PEI]$_{10}$/$P_2W_{17}V$-CNTs} in 0.5 M H_2SO_4/Na_2SO_4 buffer solution (pH = 2.5).

According to the result of the impedance spectrum, R_1 and *CPE*1 were 1682 Ω and 9.8691 × 10^{-4} F, respectively. At the interface of the tricomponent composite film [$P_2W_{17}V$-CNTs/CuO]$_{10}$/$P_2W_{17}V$-CNTs, the electric charge transmission speed constant (k) of W^{5-}/W^{6-} can be achieved by the following formula [54, 55]:

$$k = \frac{RT}{R_1 Cn^2 F^2 A} \qquad \text{(c)}$$

where n is the number of electrons transferred per electroactive species, A is the geometric area of the electrode (cm^2), and all other terms have their usual meaning. According to the above formula, the k of the tricomponent composite film was estimated to be 2.67 × 10^{-5} cm s^{-1}, while k of the two-component composite films [$P_2W_{17}V$/CuO]$_{10}$/$P_2W_{17}V$ and [$P_2W_{17}V$-CNTs/PEI]$_{10}$/$P_2W_{17}V$-CNTs were 8.94 × 10^{-6} cm s^{-1} and 2.52 × 10^{-5} cm s^{-1}, respectively. The k of the two-component composite film [$P_2W_{17}V$-CNTs/PEI]$_{10}$/$P_2W_{17}V$-CNTs is closer to that of the tricomponent composite film, suggesting that the incorporation of CNTs into the films greatly improves the conductivity of the films.

3.5 Electrochemical reduction of iodate

Before further investigations of the sensing properties of the tricomponent composite film, the optimum condition of the tricomponent composite film needs to be determined. Therefore, a series of parallel experiments were carried out to obtain the optimum condition, and the bilayer number of 10

was selected as the optimal bilayer number for further investigation of the tricomponent composite film.

Figure 7 shows the CVs of the tricomponent composite film $[P_2W_{17}V\text{-CNTs/CuO}]_{10}/P_2W_{17}V\text{-CNTs}$ in 0.5 M H_2SO_4/Na_2SO_4 solution (pH = 2.5) containing IO_3^- at different concentrations. However, it should be noted that the cathodic peak current of every coupled redox peaks of the tricomponent composite film $[P_2W_{17}V\text{-CNTs/CuO}]_{10}/P_2W_{17}V\text{-CNTs}$ gradually increased with the addition of IO_3^-, indicating that the tricomponent composite film can electrocatalytically reduce IO_3^-. The inset of Figure 7 displays the relationship between the concentration of IO_3^- and catalytic current. Clearly, the corresponding catalytic currents were enhanced linearly with the increasing concentration of IO_3^-, suggesting that this tricomponent composite film could have potential applications in the determination of IO_3^-. Moreover, the catalytic current increases at -0.52 and -0.74 V vs Ag/AgCl are much greater than the first cathodic peak, indicating that the $6e^-$ and $4e^-$ reduced states of $P_2W_{17}V$ can more effectively reduce IO_3^- than the $2e^-$ reduced form.

The catalytic efficiency of the tricomponent composite film $[P_2W_{17}V\text{-CNTs/CuO}]_{10}/P_2W_{17}V\text{-CNTs}$ for the electrocatalytic reduction of IO_3^- can be calculated according to the follow equation [56]:

$$CAT = 100\% \times [I_p(POM, substrate] - I_p[(POM)]] / I_p(POM) \quad \text{(d)}$$

where $I_p(POM, substrate)$ and $I_p(POM)$ are the peak currents at the applied potential for the reduction of POM with and without the presence of IO_3^- substrate, respectively.

At -0.52 V, when 0.5 mM IO_3^- is reduced, the electrocatalytic efficiency of the tricomponent composite film $[P_2W_{17}V\text{-CNTs/CuO}]_{10}/P_2W_{17}V\text{-CNTs}$ is 164.12% (see Fig. 5). However, the catalytic efficiencies of the two-component films $[P_2W_{17}V\text{-CNTs/PEI}]_{10}/P_2W_{17}V\text{-CNTs}$ and $[P_2W_{17}V/PEI\text{-CuO}]_{10}/P_2W_{17}V$ were 42.64% and 113.57%, respectively (the corresponding figures not shown here). It can be concluded that the incorporation of CNTs and CuO NPs into the $P_2W_{17}V$-based film greatly enhanced the electrocatalytic activity of the composite film.

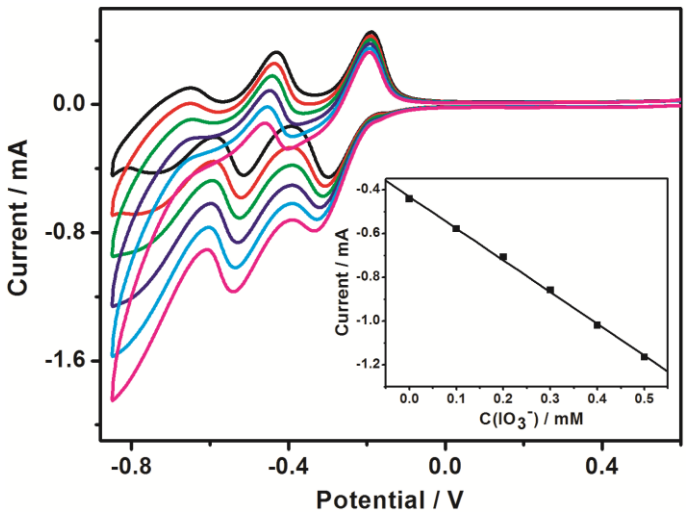

Figure 7. Cyclic voltammograms of the three-component film $\{PEI/[P_2W_{17}V\text{-CNTs/PEI-CuO}]_{10}/P_2W_{17}V\text{-CNTs}\}$ with different concentrations of IO_3^- (0, 0.1, 0.2, 0.3, 0.4 and 0.5 mM) in 0.5 M H_2SO_4/Na_2SO_4 (pH = 2.5). The inset shows the relationship between catalytic current and concentration of IO_3^-.

According to the above results, the probable electrochemical redox mechanism could be expressed as follows [57]:

$$P_2W_{17}{}^{VI}VO_{62}{}^{7-} + 2H^+ + 2e^- \rightleftharpoons H_2P_2W_{15}{}^{VI}W_2{}^{V}VO_{62}{}^{7-}$$

$$H_2P_2W_{15}{}^{VI}W_2{}^{V}VO_{62}{}^{7-} + 2H^+ + 2e^- \rightleftharpoons H_4P_2W_{13}{}^{VI}W_4{}^{V}VO_{62}{}^{7-}$$

$$3H_4P_2W_{13}{}^{VI}W_4{}^{V}VO_{62}{}^{7-} + IO_3^- \rightleftharpoons 3H_2P_2W_{15}{}^{VI}W_2{}^{V}VO_{62}{}^{7-} + 3H_2O + I^-$$

$$3H_2P_2W_{15}{}^{VI}W_2{}^{V}VO_{62}{}^{7-} + IO_3^- \rightleftharpoons 3P_2W_{17}{}^{VI}VO_{62}{}^{7-} + 3H_2O + I^-$$

$$2CuO + 2e^- + 2H^+ = Cu_2O + H_2O$$

$$3Cu_2O + IO_3^- + 12H^+ = I^- + 6Cu^{2+} + 6H_2O$$

In the electrocatalytic process, the charge transfer resistance at the surface of the electrode could be weakened by the CuO nanoparticles and carbon nanotubes with high electrical conductivity and large ratio-to-volume surface area, which promotes the electron transfer between IO_3^- and the electrode surface and significantly improves the kinetics process of iodate reduction. Meanwhile, the reduction of IO_3^- was mediated by the reduced states of $P_2W_{17}V$ and CuO (Cu(I) and Cu(II) surface states), which act as proton and electron reservoirs.

3.6 Electrochemical sensing of iodate

The sensing characteristics of the tricomponent composite film $[P_2W_{17}V$-CNTs/CuO$]_{10}/P_2W_{17}V$-CNTs was examined by amperometry. Fig. 6 shows the comparison investigations of the amperometric response of iodate for different composite films. A larger electrocatalytic current of IO_3^- reduction was observed for the tricomponent composite film $[P_2W_{17}V$-CNTs/CuO$]_{10}/P_2W_{17}V$-CNTs than those of the two-component composite films, indicating that the incorporation of CNTs and CuO NPs into the $P_2W_{17}V$-based film greatly enhanced the sensitivity of the tricomponent composite film. The response time of the tricomponent composite film, defined as the duration of the steady-state current boost from 0 to 95%, was estimated to be 2 s from Figure 8; this value is much less than that achieved by Yang's group [57] (< 6 s), Xu's group [58] (< 6 s), and Wang's group [59] (< 5 s) and is comparable to that achieved by Abdollah Salimi [60] (2 s), also confirming the faster electron transfer rate in the tricomponent composite film. It is significant to shorten the reaction time for potential application in detecting iodate.

The amperometric *i-t* curve of this as-prepared sensor was recorded upon adding iodate in sequence to a stirring 0.5 M H_2SO_4/Na_2SO_4 (pH = 2.5) solution at an applied potential of -0.5 V. With the addition of IO_3^-, the as-prepared sensor responded sensitively, and the current signal increased sharply, attaining a new steady-state current in 2 s (see Figure 9 (a)). As shown in Figure 9 (b), the steady-state current is boosted linearly upon increasing the iodate concentration and the linear range of the tricomponent composite film for detecting IO_3^- is from 1.25×10^{-7} to 1.63×10^{-4} M. The linear regression equation is $-I_{IO_3^-}(mA) = 0.14103 + 4.82 \times C_{IO_3^-}(mM)$, with a correlation coefficient of 0.9983. The detection limit was estimated to be 1.5×10^{-8} M (S/N = 3). In Table 1, the sensing characteristics of this as-prepared sensor and some others previously reported in the references are listed. These results prove that a remarkable platform for the detection of iodate could be established based on this as-prepared IO_3^- sensor.

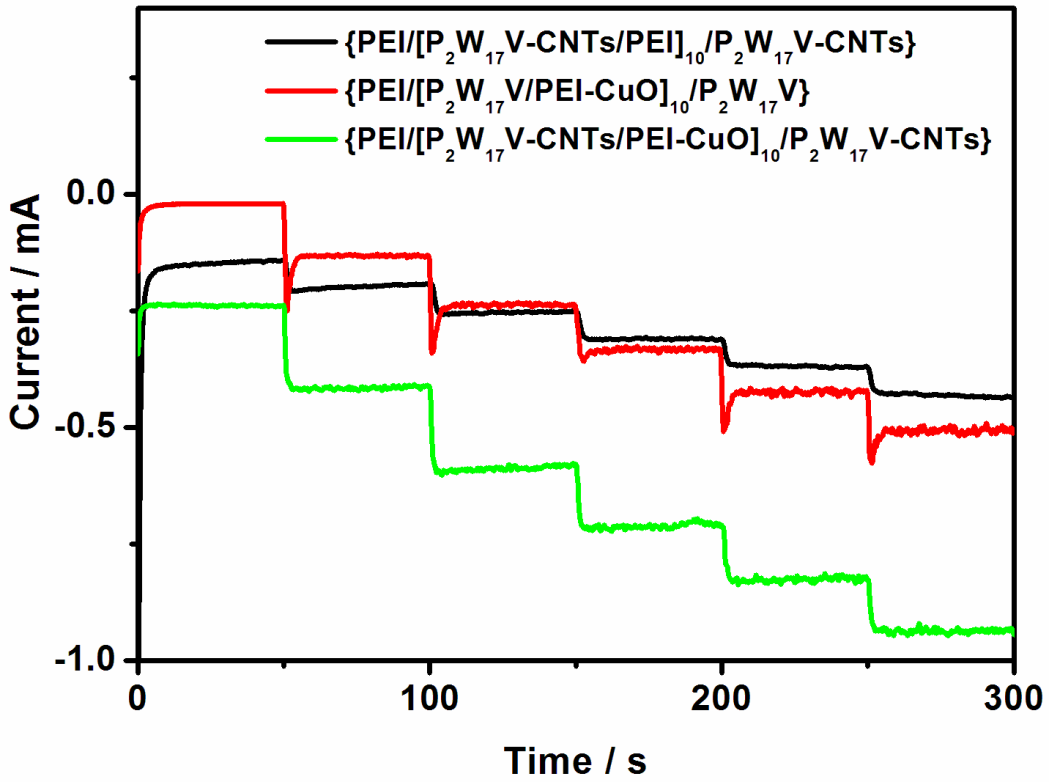

Figure 8. Comparative current-time responses at -0.5 V with 25 μM IO_3^- per 50 s for the three-component composite film {PEI/[P_2W_{17}V-CNTs/PEI-CuO]$_{10}$/P_2W_{17}V-CNTs} and two two-component composite films {PEI/[P_2W_{17}V-CNTs/PEI]$_{10}$/P_2W_{17}V-CNTs} and {PEI/[P_2W_{17}V/PEI-CuO]$_{10}$/P_2W_{17}V} in 0.5 M H_2SO_4/Na_2SO_4 buffer solution (pH = 2.5).

Table 1. Comparative characteristics of this as-prepared sensor and some other sensors for the determination of iodate.

Electrode	Potential (V)	Method	Linear range	LOD (μM)	Ref.
Zn-Al LDH/Au electrode	-0.66	Amperometric	1-2000 μM	0.25	[59]
IrOx modified GCE[a]	0.7	Flow injection amperometric	Up to 100 μM	5×10^{-3}	[60]
AMMOE[b]	-0.2	Cyclic voltammetry	1×10^{-6} to 2×10^{-4} M	0.5	[58]
PQ-modified carbon ceramic electrode	0.5	Amperometric	5×10^{-6} to 5×10^{-4} M	1.8	[57]
[P_2W_{17}V-CNTs/PEI-CuO]/ITO[c]	-0.5	Cyclic voltammetry	1.25×10^{-7} to 1.63×10^{-4} M	0.015	This work

[a] glassy carbon electrode

[b] amorphous mixed-valent molybdenum oxide film modified electrode

[c] indium tin oxide

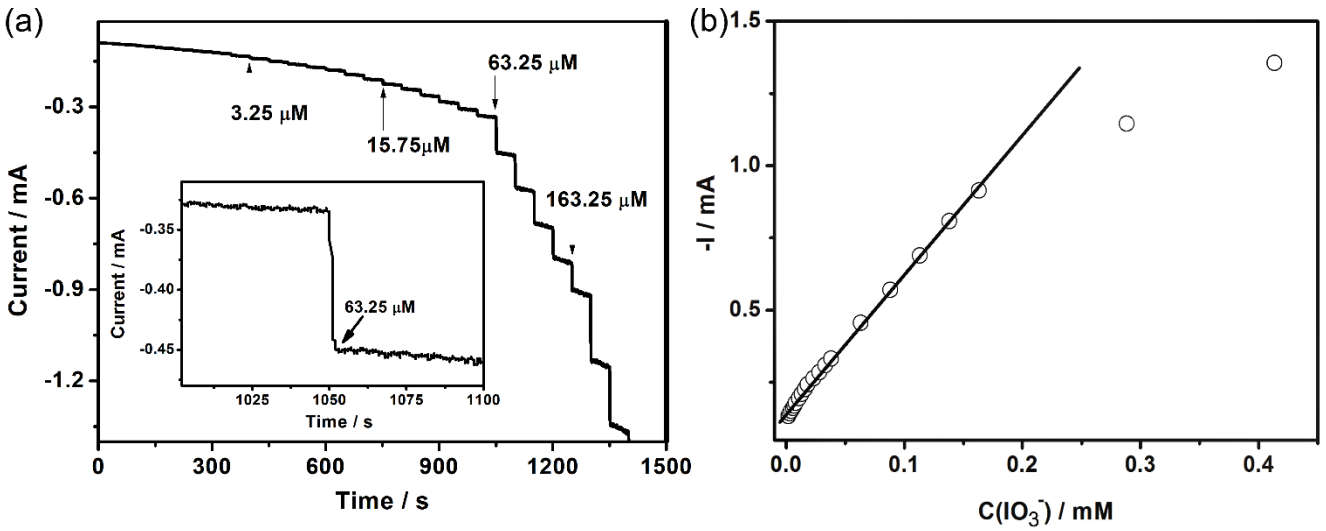

Figure 9. (a) Typical current-time curve of the {PEI/[P_2W_{17}V-CNTs/PEI-CuO]$_{10}$/P_2W_{17}V-CNTs}-modified electrode upon the successive additions of concentrations of IO_3^- at applied potential of -0.5 V vs. Ag/AgCl in 0.5 M H_2SO_4/Na_2SO_4 buffer solution (pH = 2.5) and (b) calibration plot of steady-state currents obtained at the three-component composite film {PEI/[P_2W_{17}V-CNTs/PEI-CuO]$_{10}$/P_2W_{17}V-CNTs} against concentrations of IO_3^-.

It is important to detect the content of IO_3^- accurately, rapidly and effectively in practical applications. For the sake of identifying if the sensor is influenced by the presence of common interferences in the table salt system, various foreign chemical species, which may disturb the detection of IO_3^- at the as-prepared electrode, including BrO_3^-, ClO_3^-, SO_4^{2-}, Cl^-, Ca^{2+}, Na^+, and Mg^{2+}, were added into the solution. It can be observed from Figure 10 that almost no interference was observed in the presence of possible coexisting species, certifying the impressive selectivity of this as-prepared sensor.

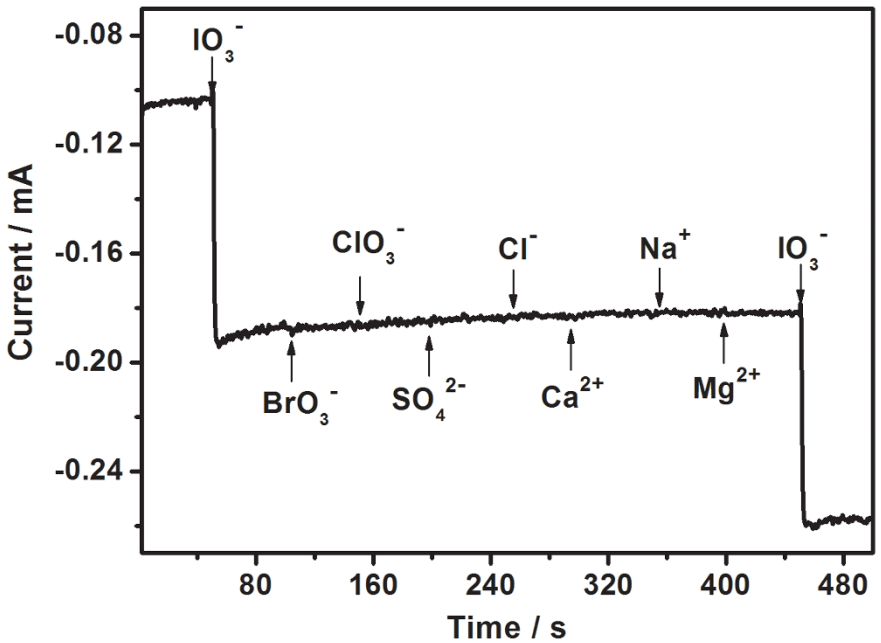

Figure 10. Amperometric response of modified electrodes in the interference of various species (0.5 M H_2SO_4/Na_2SO_4 buffer solution, pH = 2.5).

3.7 Stability and reproducibility properties of the tricomponent composite film

To determine the stability of the as-prepared sensor, a series of experiments were carried out. The characteristic absorbance at 200 and 276 nm of the tricomponent composite film $[P_2W_{17}V$-CNTs/CuO$]_{10}/P_2W_{17}V$-CNTs in the UV spectra remained unchanged in the temperature variation range from -30 °C to 150 °C (see Figure 11 (b)). The response current of the tricomponent composite film showed almost no decrease after 60 days when stored at room temperature (see Figure 11 (c)). In addition, the response current of this tricomponent composite film only dropped by 7% after 100 cycles of CV scan from -0.9 to 0.8 V in 0.5 M H_2SO_4/Na_2SO_4 solution (pH = 2.5) (see Figure 11 (a)). All of the above results testified the good stability of the tricomponent composite film. To evaluate the reproducibility of the tricomponent composite film, 6 tricomponent composite films were fabricated in a similar way. The relative standard deviation (RSD) was calculated as only 3.9%, proving its excellent reproducibility. The relatively high stability along with the excellent reproducibility makes it available for the determination of iodate.

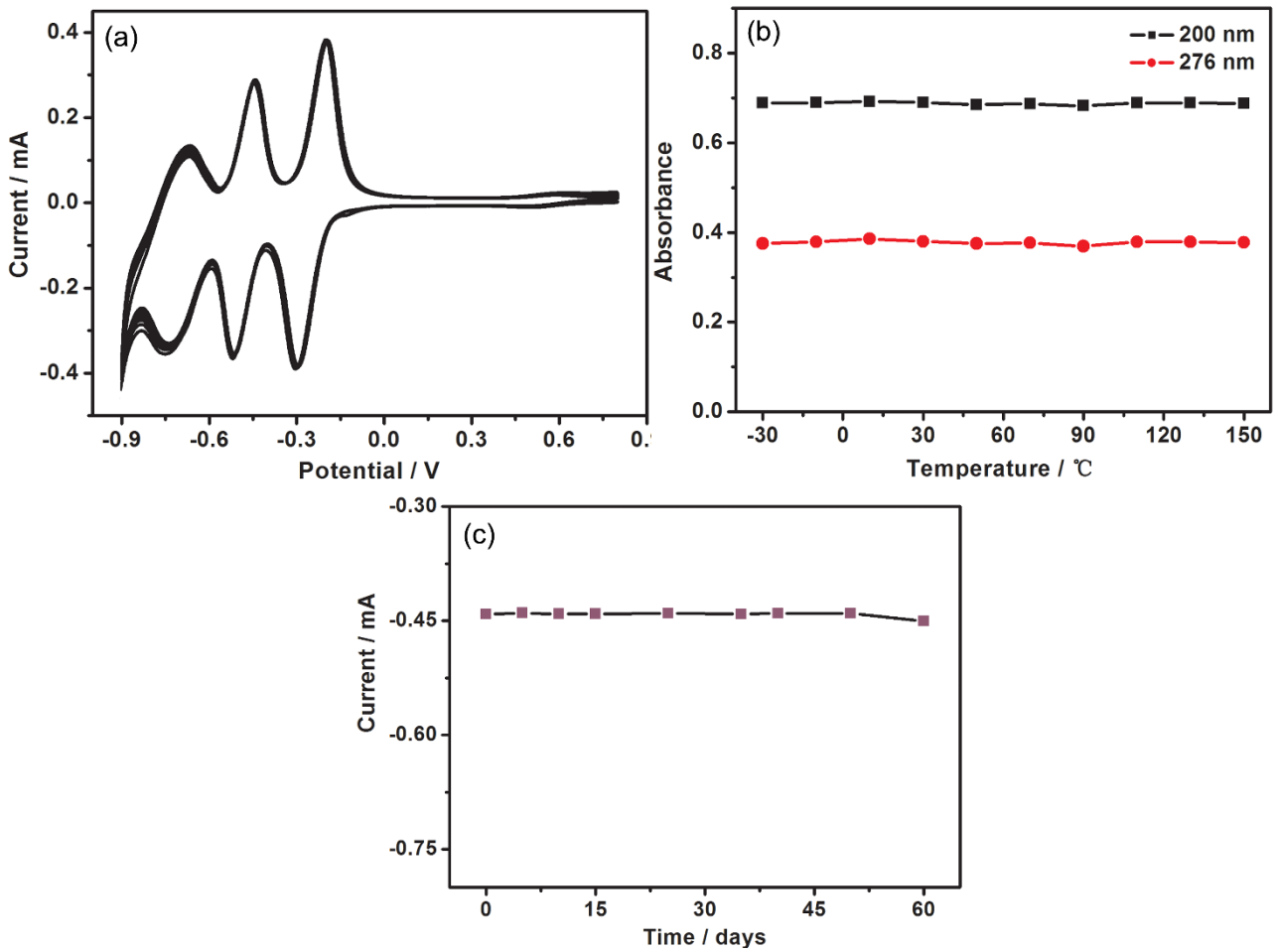

Figure 11. (a) Cyclic voltammograms of the three-component composite film {PEI/$[P_2W_{17}V$-CNTs/PEI-CuO$]_{10}/P_2W_{17}V$-CNTs} for 100 cycles in 0.5 M H_2SO_4/Na_2SO_4 buffer solution (pH = 2.5). Scan rate: 100 mV s^{-1}. (b) The absorbance of the three-component composite film {PEI/$[P_2W_{17}V$-CNTs/PEI-CuO$]_{10}/P_2W_{17}V$-CNTs} at 200 and 276 nm at different temperatures. (c) Current responses of the three-component composite film {PEI/$[P_2W_{17}V$-CNTs/PEI-CuO$]_{10}/P_2W_{17}V$-CNTs} stored at ambient conditions for 60 days at -0.5 V.

3.8 Determination of iodate in table salt

Through utilizing the amperometric response method, the as-prepared sensor was tested in table salt by measuring the concentration of iodate. Recovery studies were undertaken on the samples, and the amount of iodate standards was clarified to assess the probability of introducing the iodate sensor for analyzing iodized table salts. The results obtained are illustrated in Table 2. The achieved statistics presented that the as-prepared sensor could be used efficiently to detect iodate with an average recovery of 100.1%, showing that the dependability of the sensor presented in this work could be guaranteed.

Table 2. Results of the determination of iodate in different samples.

Samples	Content (mg/kg)	Added (mg/kg)	Found (mg/kg)	Recovery (%)
1	45.67	20	65.87	101
2	52.43	20	72.11	98.4
3	56.98	20	77.34	102.2

4. CONCLUSIONS

In summary, this work developed and introduced a new tricomponent composite film $[P_2W_{17}V$-CNTs/CuO$]_{10}/P_2W_{17}V$-CNTs electrochemical sensor to identify IO_3^- in table salt. On the basis of the obtained data, the tricomponent composite film possessed a low detection limit, broad linear range and fast amperometric response in detecting iodate. On the condition of the existence of other potential interfering species, the as-prepared iodate sensor introduced in this work has exhibited outstanding interference immunity and was successfully utilized for identifying the concentration of iodate in table salt. The excellent electrochemical performance of $[P_2W_{17}V$-CNTs/CuO$]_{10}/P_2W_{17}V$-CNTs can be attributed to the multidimensional hierarchical structure of the electrode. These achieved results indicate that the tricomponent composite film electrode holds great potential for the determination of IO_3^- in practical applications.

ACKNOWLEDGMENTS
This work was financially supported by the NSF of China (21371041, 51572063 and 21701037) and Postdoctoral Science Foundation, China (2017M611380).

References

1. M. R. Domínguez-Gonzalez, G. M. Chiocchetti, P. Herbello-Hermelo, D. Velez, V. Devesa, P. Bermejo-Barrera, *J. Agric. Food Chem*., 65 (2017) 8435-8442.
2. F. Chatraei, H. R. Zare, *Mater. Sci. Eng. C Mater. Biol. Appl*., 33 (2013) 721-726.
3. Z. Huang, Q. Subhani, Z. Zhu, W. Guo, Y. Zhu, *Food Chem*., 139 (2013) 144-148.
4. Z. Huang, Z. Zhu, Q. Subhani, W. Guo, Y. Zhu, *J. Chromatogr. A*, 1251 (2012) 154-159.

5. S. Zhang, K. A. Schwehr, Y. F. Ho, C. Xu, K. A. Roberts, D. I. Kaplan, R. Brinkmeyer, C. M. Yeager, P. H. Santschi, *Environ. Sci. Technol*., 44 (2010) 9042-9048.
6. R. Li, P. Xu, J. Fan, J. Di, Y. Tu, J. Yan, *Anal. Chim. Acta*, 827 (2014) 80-85.
7. S. S. Borges, J. S. Peixoto, M. A. Feres, B. F. Reos, *Anal. Chim. Acta*, 668 (2010) 3-7.
8. N. Choengchan, K. Uraisin, K. Choden, W. Veerasai, K. Grudpan, D. Nacapricha, *Talanta*, 58 (2002) 1195-1201.
9. M. V. Salvia, G. Salassa, F. Rastrelli, F. Mancin, *J. Am. Chem. Soc*., 137 (2015) 11399-11406.
10. Y. B. Ding, W. H. Zhu, Y. S. Xie, *Chem. Rev*., 117 (2017) 2203-2256.
11. W. Sun, S. G. Guo, C. Hu, J. L. Fan, X. J. Peng, *Chem. Rev*., 116 (2016) 7768-7817.
12. J. H. Cheng, X. F. Ma, Y. H. Zhang, J. Y. Liu, X. G. Zhou, H. F. Xiang, *Inorg. Chem*., 53 (2014) 3210-3219.
13. C. M. Rudzinski, A. M. Young, D. G. Nocera, *J. Am. Chem. Soc*., 124 (2002) 1723-1727.
14. X. Zhou, S. Y. Lee, Z. C. Xu, J. Y. Yoon, *Chem. Rev*., 115 (2015) 7944-8000.
15. M. H. Lee, Z. G. Yang, C. W. Lim, Y. H. Lee, S. D. Bang, C. Kang, J. S. Kim, *Chem. Rev*., 113 (2013) 5071-5109.
16. S. Wang, G. Yang, *Chem. Rev*., 115 (2015) 4893-4962.
17. 17. Y. Kim, S. Shanmugam, *ACS Appl. Mater. Interfaces*, 5 (2013) 12197-12204.
18. S. S. Wang, G. Y. Yang, *Chem. Rev*., 115 (2015) 4893-4962.
19. Y. Ji, L. Huang, J. Hu, C. Streb, Y. F. Song, *Energy Environ. Sci*., 8 (2015) 776-789.
20. G. H. Dong, D. B. Xia, Y. L. Yang, L. Sheng, T. L. Ye, R. Q. Fan, *ACS Appl. Mater. Interfaces*, 9 (2017) 2378-2386.
21. J. Gonzalez, J. A. Coca-Clemente, A. Molina, E. Laborda, J. M. Gomez-Gil, L. A. Rincon, *ACS Catal*., 7 (2017) 1501-1511.
22. C. X. Li, K. P. O′ Halloran, H. Y. Ma, S. L. Shi, *J. Phys. Chem. B*, 113 (2009) 8043-8048.
23. C. X. Li, X. G. Wang, H. Y. Ma, F. P. Wang, Y. Gu, *Electroanal*., 20 (2008) 1110-1115.
24. D. M. Fernandes, A. Teixeira, C. Freire, *Langmuir*, 31 (2015) 1855-1865.
25. D. M. Fernandes, A. D. S. Barbosa, J. Oires, S. S. Balula, L. Cunha-Silva, C. Freire, *ACS Appl. Mater. Interfaces*, 5 (2013) 13382-13390.
26. W. Zhu, W. Zhang, S. Li, H. Ma, W. Chen, H. Pang, *Sensor. Actuat. B*, 181 (2013) 773-781.
27. C. Zhou, S. Li, W. Zhu, H. Pang, H. Ma, *Electrochim. Acta*, 113 (2013) 454-463.
28. S. Li, H. Ma, K. O′ Halloran, H. Pang, H. Ji, *Electrochim. Acta*, 108 (2013) 717-726.
29. D. Zhang, H. Ma, Y. Chen, H. Pang, Y. Yu, *Electrochim. Acta*, 792 (2013) 35-44.
30. X. Zhang, J. S. Luo, P. Y. Tang, J. R. Morante, J. Arbiol, C. L. Xu, Q. F. Li, J. Fransaer, *Sensors and Actuators B*, 254 (2018) 272-281.
31. J. Huang, Y. Zhu, X. Yang, W. Chen, Y. Zhou, C. Li, *Nanoscale*, 7(2) (2015) 559-569.
32. Z. Li, Y. Chen, Y. Xin, Z. Zhang, *Sci. Rep*., 5 (2015) 16115-16123.
33. D. Jiang, Q. Liu, K. Wang, J. Qian, X. Dong, Z. Yang, X. Du, B. Qiu, *Biosens. Bioelectron*, 54 (2014) 273-278.
34. R. Akter, M. A. Rahman, C. K. Rhee, *Anal. Chem*., 84 (2012), 6407-6415.
35. Z. Weng, W. Liu, L. C. Yin, R. P. Fang, M. Li, E. I. Altman, Q. Fan, F. Li, H. M. Cheng, H. L. Wang, *Nano Lett*., 15 (2015) 7704-7710.
36. X. L. Li, W. Liu, M. Y. Zhang, Y. R. Zhong, Z. Weng, Y. Y. Mi, Y. Zhou, M. Li, J. J. Cha, Z. Y. Tang, H. Jiang, X. M. Li, H. L. Wang, *Nano Lett*., 17 (2017) 2057-2063.
37. M. Sun, G. Zhang, Y. H. Qin, M. J. Cao, Y. Liu, J. H. Li, J. H. Qu, H. J. Liu, *Environ. Sci. Technol*., 49 (2015) 9289-9297.
38. N. Wester, S. Sainio, T. Palomäki, D. Nordlund, V. K. Singh, L. S. Johansson, J. Koskinen, T. Laurila, *J. Phys. Chem. C*, 121 (2017) 8153-8164.
39. Y. Zhang, X. Bo, A. Nsabimana, A. Munyentwali, C. Han, M. Li, *Biosens. Bioelectron*., 66 (2015) 191-197.
40. S. J. Huo, Z. Weng, Z. S. Wu, Y. R. Zhong, Y. S. Wu, J. H. Fang, H. L. Wang, *ACS Appl. Mater.*

Interfaces, 9 (2017) 28519-28526.
41. S. Pal, M. Sahoo, V. T. Veettil, K. K. Tadi, A. Ghosh, P. Satyam, R. K. Biroju, P. M. Ajayan, S. K. Nayak, T. N. Narayanan, *ACS Catal*., 7 (2017) 2676-2684.
42. J. X. Shen, Z. Yang, M. Z. Ge, P. Li, H. G. Nie, Q. R. Cai, C. C. Gu, K. Q. Yang, S. M. Huang, *ACS Appl. Mater. Interfaces*, 8 (2016) 17284-17291.
43. B. Seo, Y. J. Sa, J. Woo, K. Kwon, J. Park, T. J. Shin, H. Y. Jeong, S. H. Joo，*ACS Catal*., 6 (2016) 4347-4355.
44. Y. P. Song, H. F. Hu, M. Feng, H. B. Zhan, *ACS Appl. Mater. Interfaces*, 7 (2015) 25793-25803.
45. N. Zhou, Q. D. An, Z. Y. Xiao, S. R. Zhai, Z. Shi, *ACS Sustainable Chem. Eng*., 5 (2017) 5394-5407.
46. M. Abbessi, R. Contant, R. Thouvenot, G. Hervé, *Inorg. Chem*., 30 (1991) 1695-1702.
47. B. Keita, E. Abdeljalil, L. Nadjo, B. Avisse, R. Contant, J. Canny, M. Richet, *Electrochem. Commun*., 2 (2000) 145-149.
48. R. Ahmad, M. Vaseem, N. Tripathy, Y. B. Hahn, *Anal. Chem*., 85 (2013) 10448-10454.
49. C. X. Li, K. P. O′ Halloran, H. Y. Ma, S. L. Shi, *J. Phys. Chem. B,* 113 (2009) 8043-8048.
50. I. Creaser, M. C. Heckel, R. J. Neitz, M. T. Pope, *Inorg. Chem*., 32 (1993) 1573-1578.
51. F. Caruso, D. G. Kurth, D. Volkmer, M. J. Koop, A. Muller, *Langmuir*, 14 (1998) 3462-3465.
52. S. Q. Liu, D. G. Kurth, B. Bredenkotter, D. Volkmer, *J. Am. Chem. Soc*., 124 (2002) 12279-12287.
53. B. Keita, I. M. Mbomekalle, L. Nadjo, P. Oliveira, A. Ranjbari, R. Contant, *CR. Chim*., 8 (2005) 1057-1066.
54. E. Sabatani, I. Rubinstein, *J. Phys. Chem*, 91 (1987) 6663-6669.
55. L. Chen, L. Tian, L. Liu, X. F. Tian, W. B. Song, H. D. Xua, X. H. Wang, *Sensor. Actuat. B*, 110 (2005) 271-278.
56. A. M. Khenkin, L. Weiner, Y. Wang, R. Neumann, *J. Am. Chem. Soc*., 123 (2001) 8540-8542.
57. Z. Yang, P. Wang, W. Zhang, G. Zhu, *Fresenius J. Anal. Chem*., 371 (2001) 337-341.
58. L. Tian, L. Liu, L. Chen, N. Lu, H.D. Xu, *Sens. Actuators B*, 105 (2005) 484-489.
59. M. Li, F. Ni, Y. Wang, S. Xu, D. Zhang, L. Wang, *Appl. Clay Sci*., 46 (2009) 396-400.
60. A. Salimi, R. Hallaj, B. Kavosi, B. Haqiqhi, *Anal. Chim. Acta*, 661 (2010) 28-34.